TECHNICAL REPORT NO. TR-763

A NUMERICAL STUDY OF THE LAMINAR NEAR-WAKE OF AN AXISYMMETRIC BODY IN A SUPERSONIC FLOW

(Final Report)

By Charles Ruger

for

U. S. Army Missile Command
Redstone Arsenal, Alabama

This research was supported by the Advanced Research Projects Agency of the Department of Defense and was monitored by the U. S. Army Missile Command under Contract DAAH01-69-C-0792.

This research was sponsored by the Advanced Research Projects Agency, Order Nr. 1310.

October 1971

Unclassified

Security Classification

DOCUMENT CONTROL DATA - R & D

(Security classification of title, body of abstract and indexing annotation must be entered when the overall report is classified)

1. ORIGINATING ACTIVITY (Corporate author) General Applied Science Laboratories, Inc. Westbury, New York	2a. REPORT SECURITY CLASSIFICATION U 2b. GROUP N/A

3. REPORT TITLE
A Numerical Study of the Laminar Near-Wake of an Axisymmetric Body in a Supersonic Flow

4. DESCRIPTIVE NOTES (Type of report and inclusive dates)
Final Report

5. AUTHOR(S) (First name, middle initial, last name)
Charles Ruger

6. REPORT DATE October 1971	7a. TOTAL NO. OF PAGES 92	7b. NO. OF REFS 9
8a. CONTRACT OR GRANT NO DAAH01-69-C-0792 b. PROJECT NO c. ARPA Order Nr. 1310 d.	9a. ORIGINATOR'S REPORT NUMBER(S) GASL TR-763 9b. OTHER REPORT NO(S) (Any other numbers that may be assigned this report)	

10. [redacted]

11. SUPPLEMENTARY NOTES

12. SPONSORING MILITARY ACTIVITY
Advanced Research Projects Agency
Washington, D. C.

13. ABSTRACT A numerical solution of the laminar, steady near wake of an axisymmetric body in supersonic flow is developed. The body considered is a spherically capped cylinder with a truncated base. The full set of compressible partial differential equations are solved.

The numerical approach is a two-step time dependent finite difference procedure similar to that used by Cheng and Allen in two-dimensions. The scheme is the elimination of the viscosity dependent stability condition fo the time dependent solution. A variable mesh grid system is included to provide higher resolution in areas of flow nonuniformity and both the equation system and the finite differencing are done in conservation form. The difference forms at the boundaries are obtained by means of telescoping with the internal difference forms.

A series of numerical examples were calculated on a CDC 6600 computer with both a coarse and fine mesh configuration for various free stream Reynolds numbers. Convergent, steady state solutions were obtained which exhibited definite recirculation regions and showed evidence of recompression shocks. Restrictions on the Reynolds number for a given mesh size were investigated, as was the relationship between solution curvatures and mesh size.

DD FORM 1 NOV 1473

Unclassified

Security Classification

14. KEY WORDS	LINK A		LINK B		LINK C	
	ROLE	WT	ROLE	WT	ROLE	WT
Near Wake						
Finite Difference						
Numerical Solution						
Flow Fields						
Supersonic Flow						

TECHNICAL REPORT NO. TR-763

A NUMERICAL STUDY OF THE LAMINAR NEAR-WAKE OF AN AXISYMMETRIC BODY IN A SUPERSONIC FLOW

(Final Report)

By Charles Ruger

for

U. S. Army Missile Command
Redstone Arsenal, Alabama

This research was supported by the Advanced Research Projects Agency of the Department of Defense and was monitored by the U. S. Army Missile Command under Contract DAAH01-69-C-0792

This research was sponsored by the Advanced Research Projects Agency, Order Nr. 1310.

by

General Applied Science Laboratories, Inc.
An Affiliate of The Marquardt Company
Merrick and Stewart Avenues
Westbury, New York 11590

October 27, 1971

Approved by: L. M. Nucci
Louis M. Nucci
President

ABSTRACT

A numerical solution of the laminar, steady near wake of an axisymmetric body in supersonic flow is developed. The body considered is a spherically capped cylinder with a truncated base. The full set of compressible partial differential equations are solved.

The numerical approach is a two-step time dependent finite difference procedure similar to that used by Cheng and Allen in two-dimensions. The primary feature of this scheme is the elimination of the viscosity dependent stability condition for the time dependent solution. A variable mesh grid system is included to provide higher resolution in areas of flow nonuniformity and both the equation system and the finite differencing are done in conservation form. The difference forms at the boundaries are obtained by means of telescoping with the internal difference forms.

A series of numerical examples were calculated on a CDC 6600 computer with both a coarse and fine mesh configuration for various free stream Reynolds numbers. Convergent, steady state solutions were obtained which exhibited definite recirculation regions and showed evidence of recompression shocks. Restrictions on the Reynolds number for a given mesh size were investigated, as was the relationship between solution curvatures and mesh size.

TABLE OF CONTENTS

SECTION	PAGE
INTRODUCTION	1
MODEL PROBLEM AND INTERNAL NUMERICAL SCHEME	3
Configuration	3
Spatial Differencing	3
Time Differencing	8
BOUNDARIES	17
Upstream	17
Body Wall and Base	17
Centerline	24
Downstream	30
Upper Boundary	31
NUMERICAL RESULTS	36
Computer Program	36
Input Data	37
Time Step and Steady State Criteria	39
Numerical Examples	40
Coarse Mesh Solutions	40
Fine Mesh Solutions	42
SUMMARY	45
REFERENCES	47
FIGURES	48

TABLE OF CONTENTS (continued)

SECTION		PAGE
APPENDIX I -	SPATIAL DIFFERENCING FUNCTIONS FOR BOUNDARIES	I-1
APPENDIX II-	COMPUTER PROGRAM - INPUT-OUTPUT DESCRIPTION	II-1
APPENDIX III -	A FEASIBILITY STUDY FOR TURBULENT COMPRESSIBLE FLOW ANALYSIS	III-1

NOMENCLATURE

a	General coefficients in difference forms and constant in Sutherlands Law
d	Constant in isentropic pressure density relationship
e	Energy normalized by free stream value
$\bar{e}$	Normalized energy resulting from first iteration step
f	General function in difference forms
F_1, F_2, F_3, F_4	Functions appearing on right hand side of difference form of continuity, axial momentum, radial momentum and energy equations (Equations 8 and 9).
$\bar{F}$	Portions of F functions consisting of non-central parts of twice spatially differenced diffusive terms
$\bar{F}_1$, $\bar{F}_2$, $\bar{F}_3$, $\bar{F}_4$	$\bar{F}$ functions for continuity, axial momentum, radial momentum and energy equations
G	Functions containing updated central portions of twice spatially differenced diffusive terms
G_2, G_3, G_4	G functions appearing in denominators of difference form of axial momentum, radial momentum and energy equations.
H	Portions of F functions which are not twice spatially differenced diffusive terms and constant stagnation enthalpy along streamline
k	Thermal conductivity normalized by free stream value
$\bar{k}$	Normalized thermal conductivity resulting from first iteration step
M	Mach number

$\bar{M}_\infty = u_\infty^2/e_\infty$

$\hat{M}_\infty = 1/\gamma_\infty M_\infty^2$

P Normalized static pressure

Pr Prandtl number

$q = (u^2+v^2)\bar{M}_\infty/2$

r Radial coordinate normalized by base half height

R Gas constant

Re Reynolds number based on base half height

Re_Δ Reynolds number based on mesh size

t Time normalized by base half height $\div u_\infty$

u Axial velocity component normalized by free stream velocity

$\bar{u}$ Normalized axial velocity resulting from first iteration step

v Radial velocity component normalized by free stream velocity

$\bar{v}$ Normalized radial velocity resulting from first iteration step

x Axial coordinate normalized by base half height

$X = (\gamma - 1)/(\gamma_\infty - 1)$

α Ratio of adjacent axial mesh sizes

β Ratio of adjacent radial mesh sizes

γ Ratio of specific heats

δ Ratio of mesh sizes Δr_{m+2} and Δr_m

Δr Radial mesh size

Δt Normalized time step

Δx Axial mesh size

ϵ Limiting value for stability criteria

$\zeta = (\gamma-1)R/(\gamma_\infty-1)R_\infty$

$\bar{\zeta}$ Value of ζ resulting from first iteration step

θ Flow deflection along upper boundary

μ Fluid viscosity normalized by free stream value

$\bar{\mu}$ Normalized viscosity resulting from first iteration step

ν Kinematic viscosity

ρ Density normalized by free stream value

$\bar{\rho}$ Normalized density resulting from first iteration step

Subscripts

A Starting point of upper boundary characteristics extrapolation

B Intersection point of first family characteristic line and upper boundary line

c Centerline value

C Intersection point of streamline and $x = x_A$ line

m Radial mesh point index

M Upper boundary line index

n Axial mesh point index

N Downstream boundary line index

w Body wall value

∞ Free stream value, ahead of bow shock

0 Point one half mesh from wall

1 Point one and one half meshes from wall or point one mesh from $\mathcal{L}$

2 Point two meshes from $\mathcal{L}$

Superscript

j Time step index

ACKNOWLEDGMENTS

The author wishes to express his sincere thanks to Dr. Frank Lane for his essential guidance during the course of this work. Acknowledgment is also given to Mr. David Wicks who did the computer programming and contributed Appendix II, and Mr. Geoffrey Maltin who studied the feasibility of extending this method to turbulent flow, in Appendix III.

INTRODUCTION

This work aims at treating the laminar,* steady, axisymmetric near wake of a body with a cylindrical base traveling at supersonic velocity by the numerical solution of the full set of compressible partial differential equations governing the motion. This approach eliminates the need for approximations, such as the boundary layer approximation and the patching of separate regions where different approximations are made. Numerical solutions also have the advantage that they give all the details of the flow, while methods such as approximate integral solutions do not. In theory at least, numerical solutions can be used to check their own accuracy by making calculations at successively smaller grid sizes.

The differential equations under consideration are the full compressible Navier Stokes equations in axisymmetric coordinates and the numerical scheme consists of a two-step time-dependent finite difference procedure. Several such techniques have been considered,[1] but the most promising appears to be the approach of Cheng[3] and Allen.[4,5] Allen[4] has treated the two-dimensional case, utilizing a uniform, but non-square mesh and assuming constant viscosity and conductivity and simplified outside flow. The present work attempts to extend this to an axisymmetric configuration and realistic outer flow. Moreover, a nonuniform mesh is being introduced to give greater resolution in the high-gradient regions.

The other possibly competitive techniques[1,2] have been considered and discarded. Schemes with viscosity dependent stability criteria, such as Reference 1, appear to be susceptible to numerical difficulties in the body wall and base regions, those difficulties taking the form of very small or even negative density values as the time-evolution of the flow computation proceeds. Such phenomena

* The feasibility of extending this work to turbulent flows is discussed in Appendix III.

play havoc with the stability of the computation. The scheme of Reference 2 was found to have stability difficulties at the outflow and possibly the upper boundaries.[4] We are attempting to take advantage of the numerical discovery by Cheng and Allen, of these pitfalls and of the techniques which appear to avoid their occurrence.

MODEL PROBLEM AND INTERNAL NUMERICAL SCHEME

Configuration

The type of axisymmetric body being considered is shown in Figure 1. Note that the base section is cylindrical, which is a simplifying assumption of this program. The calculation domain being considered is ABCFGHJA. The inflow boundary AC is set back upstream of the base HJ to permit upstream influence in the boundary layer to occur. The bow shock and the outer region CDEF are computed by the method of characteristics, where characteristic BF defines the limit of influence of the boundary layer up to point A. This characteristics calculation is used to obtain the inviscid portion of the flow field upstream of the line ABCD. The viscous region upstream of line AB is obtained from a boundary layer calculation[6], which is started far upstream of point A with an initial step profile. The downstream boundary GF is located where the flow has become entirely supersonic. The data on this boundary is obtained by an extrapolation from the calculated flow field.

Spatial Differencing

Since a steady state solution is the objective, it is necessary to develop a consistent set of spatial differencing approximations for the steady state terms. The flow field being considered is expected to contain discontinuities such as shocks. Therefore it is desirable as pointed out by Lax, Wendroff et al.[7] to use the conservation form of the differential and difference equations. In principle the conservation form of the Navier Stokes equations in three-dimensional cartesian coordinates can be retained under a transformation to three-dimensional cylindric

coordinates.[8] However, when this conservation-preserving set of equations is reduced by the assumption of axisymmetry, circumferential terms and derivatives vanish except for a circumferential normal stress term in the radial momentum equation. This term cannot be put into conservation form but this should not be disastrous since there will be no jumps across discontinuities in the circumferential direction. The resulting non-dimensionalized, unsteady continuity, axial and radial momentum and energy equations are:

$$(\rho r)_t + (\rho r u)_x + (\rho r v)_r = 0$$

$$(\rho r u)_t + \left[\rho r u v - \frac{r\mu}{Re_\infty}(v_x + u_r)\right]_r + \left[\rho r(u^2 + \hat{M}_\infty e X) - \frac{4}{3}\frac{r\mu}{Re_\infty} u_x + \frac{2}{3}\frac{r\mu}{Re_\infty}\left(v_r + \frac{v}{r}\right)\right]_x = 0$$

$$(\rho r v)_t + \left[\rho r u v - \frac{r\mu}{Re_\infty}(v_x + u_r)\right]_x + \left[\rho r(v^2 + \hat{M}_\infty e X) - \frac{4}{3}\frac{r\mu}{Re_\infty} v_r + \frac{2}{3}\frac{r\mu}{Re_\infty}\left(u_x + \frac{v}{r}\right)\right]_r - \rho \hat{M}_\infty e X - \frac{2}{3}\frac{\mu}{Re_\infty}(v_r + u_x) + \frac{4}{3}\frac{\mu}{Re_\infty}\frac{v}{r} = 0 \qquad (1)$$

$$[\rho r(e+q)]_t + \left\{\rho ru(\gamma e+q) - \frac{\gamma_\infty}{P_r Re_\infty}[rk(\zeta e)_x]\right.$$

$$\left. - \frac{\bar{M}_\infty}{Re_\infty}\left[\frac{2}{3} r\mu(u^2)_x + \frac{r\mu}{2}(v^2)_x - \frac{2}{3} r\mu uv_r + r\mu vu_r - \frac{2}{3}\mu uv\right]\right\}_x$$

$$+ \left\{\rho rv(\gamma e+q) - \frac{\gamma_\infty}{P_r Re_\infty}[rk(\zeta e)_r]\right.$$

$$- \frac{\bar{M}_\infty}{Re_\infty}\left[\frac{2}{3} r\mu(v^2)_r + \frac{r\mu}{2}(u^2)_r - \frac{2}{3} r\mu vu_x\right.$$

$$\left.\left. + r\mu uv_x - \frac{2}{3}\mu v^2\right]\right\}_r = 0$$

(1) concluded

where

$$X = \frac{\gamma - 1}{\gamma_\infty - 1}$$

$$\zeta = \left(\frac{\gamma-1}{\gamma_\infty - 1}\right)\frac{R_\infty}{R}$$

$$q = (u^2 + v^2)\frac{\bar{M}_\infty}{2}$$

$$\bar{M}_\infty = u_\infty^2/e_\infty$$

$$\hat{M}_\infty = \frac{1}{\gamma_\infty M_\infty^2}$$

γ is the ratio of specific heats, R is the gas constant, Re the Reynolds number, Pr the Prandtl number, and all flow variables are normalized by their values in the free stream, which are denoted by the subscript ∞.

Since localized areas of interest such as boundary layers, shear layers, and shocks, are present in the flow field, a non-uniform-grid finite difference scheme is desirable. This will allow use of a fine mesh in these special areas, while a coarser grid can be used in other areas preventing machine time from becoming unwieldy.

A second order accurate centered finite difference scheme for a variable mesh will yield approximations for both the first and second derivatives which depend upon the values of the function at three grid points; the one at which the derivative is required and the two adjacent points. If such a scheme is applied to the steady terms of the continuity equation, for instance, it is easily shown that the inclusion of the central term in the first difference approximation yields a difference equation which is not in conservation form. Therefore, a first order accurate, centered difference scheme, which yields a set of difference equations in conservation form, is used. For two axial steps with a length ratio α the first and second differences of a function f are

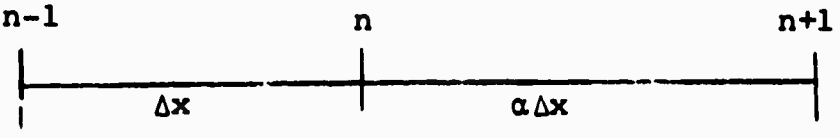

$$(f_x)_n = \frac{f_{n+1} - f_{n-1}}{(\alpha+1)\Delta x} \tag{2}$$

$$(f_{xx})_n = 2\,\frac{f_{n+1} - (1+\alpha)f_n + \alpha\, f_{n-1}}{\alpha(\alpha+1)\Delta x^2} \tag{3}$$

with similar expressions for the radial difference with the radial step size ratio β replacing α.

Taylor series expansions of f_{n+1} and f_{n-1} about f_n show the error of the above schemes with respect to the error of the second order central scheme for a uniform mesh to be, respectively

$$\frac{3(\alpha-1)}{\Delta x} \quad \frac{(f_{xxx})_n}{(f_{xxx})_n} \tag{4}$$

and

$$\frac{4(\alpha-1)}{\Delta x} \quad \frac{(f_{xxx})_n}{(f_{xxxx})_n}$$

Therefore, the accuracy of the present scheme can be controlled by keeping the relative grid spacing α close to unity.

Since variable viscosity and heat conductivity are being considered, difference approximations for terms of the form $(af_x)_x$ and $(af_x)_r$ will be required. These can be obtained by successive applications of the first difference expression (2)

$$\begin{aligned}[(af_x)_x]_{m,n} = \{ &(a_{m,n+1} + a_{m,n})\, f_{m,n+1} \\ &- [a_{m,n+1} + (1+\alpha)\, a_{m,n} + \alpha a_{m,n-1}] f_{m,n} \\ &+ \alpha (a_{m,n} + a_{m,n-1})\, f_{m,n-1} \} \Big/ \alpha(\alpha+1)\Delta x^2 \end{aligned} \tag{5}$$

A similar expression for $(af_r)_r$ can be obtained by replacing α by β, Δx by Δr, and interchanging m and n, where β is the ratio of successive mesh intervals in the radial direction. The cross derivative expressions are

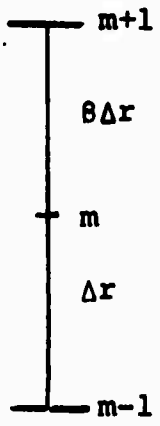

$$[(af_x)_r]_{m,n} = [a_{m+1,n}(f_{m+1,n+1} - f_{m+1,n-1}) - a_{m-1,n}(f_{m-1,n+1} - f_{m-1,n-1})] \Big/ (\alpha+1)(\beta+1)\Delta x \Delta r \quad (6)$$

$$[(af_r)_x]_{m,n} = [a_{m,n+1}(f_{m+1,n+1} - f_{m-1,n+1}) - a_{m,n-1}(f_{m+1,n-1} - f_{m-1,n-1})] \Big/ (\sigma+1)(\beta+1)\Delta x \Delta r \quad (7)$$

Time Differencing

The form of the spatial difference influences the choice of a time differencing scheme through stability considerations. One stable scheme consistent with the above spatial differencing is the two-step scheme of Brailovskaya.[1] There are two stability criteria on time step associated with this scheme, one linearly dependent upon the spatial step size ($\Delta t \leq \frac{\Delta x}{c}$) and the other proportional to the square of the spatial step size divided by the kinematic viscosity ($\Delta t \leq \frac{\Delta x^2}{4\nu}$). In the present problem, there is a large expansion of the flow around the base and the density in the base region becomes small. This will result in a large kinematic viscosity and severely limits the time step results.

Allen[4] has considered a modification of the Brailovskaya scheme which removes the diffusion dependent stability criteria. The modification consists of writing the independent variables appearing in central terms of twice spatially differenced diffusive terms at the updated time level and combining them with the time differenced unsteady terms to solve for the independent variables at the new time level. This works because we are only interested in the steady state solution and how we get there, i.e., the time evolution of the solution is irrelevant.

Then the time difference scheme for the present differential equations can be written in two steps:

1)

$$\bar{\rho}^{j+1}_{m,n} = \rho^{j}_{m,n} + \frac{\Delta t}{r_m} F_1(\rho^j, u^j, v^j)_{m,n}$$

$$\bar{u}^{j+1}_{m,n} = \frac{\left[(\rho u)^{j}_{m,n} + \frac{\Delta t}{r_m} F_2(\rho^j, u^j, v^j, e^j, \mu^j, X^j)_{m,n}\right]}{\bar{\rho}^{j+1}_{m,n} + \frac{\Delta t}{r_m Re_\infty} G_2(\mu^j)_{m,n}} \qquad (8)$$

$$\bar{v}^{j+1}_{m,n} = \frac{\left[(\rho v)^{j}_{m,n} + \frac{\Delta t}{r_m} F_3(\rho^j, u^j, v^j, e^j, \mu^j, X^j)_{m,n}\right]}{\bar{\rho}^{j+1}_{m,n} + \frac{\Delta t}{r_m Re_\infty} G_3(\mu^j)_{m,n}}$$

$$\bar{e}^{j+1}_{m,n} = \frac{\left\{\left[\rho(e+q)\right]^{j}_{m,n} - (\bar{\rho}\bar{q})^{j+1}_{m,n} + \frac{\Delta t}{r_m} F_4(\rho^j, u^j, v^j, e^j, \mu^j, k^j, \bar{u}^{j+1}, \bar{v}^{j+1})_{m,n}\right.}{\bar{\rho}^{j+1}_{m,n} + \frac{\gamma_\infty}{P_r Re_\infty} \frac{\Delta t}{r_m} G_4(k^j)_{m,n}}$$

2)

$$\rho^{j+1}_{m,n} = \rho^{j}_{m,n} + \frac{\Delta t}{r_m} F_1(\bar{\rho}^{j+1}, \bar{u}^{j+1}, \bar{v}^{j+1})_{m,n}$$

$$u^{j+1}_{m,n} = \frac{\left[(\rho u)^{j}_{m,n} + \frac{\Delta t}{r_m} F_2(\bar{\rho}^{j+1}, \bar{u}^{j+1}, \bar{v}^{j+1}, \bar{e}^{j+1}, \bar{\mu}^{j+1}, \bar{X}^{j+1})_{m,n}\right]}{\rho^{j+1}_{m,n} + \frac{\Delta t}{r_m Re_\infty} G_2(\bar{\mu}^{j+1})_{m,n}}$$

$$v^{j+1}_{m,n} = \frac{\left[(\rho v)^{j}_{m,n} + \frac{\Delta t}{r_m} F_3(\bar{\rho}^{j+1}, \bar{u}^{j+1}, \bar{v}^{j+1}, \bar{e}^{j+1}, \bar{\mu}^{j+1}, \bar{X}^{j+1})_{m,n}\right]}{\rho^{j+1}_{m,n} + \frac{\Delta t}{r_m Re_\infty} G_3(\bar{\mu}^{j+1})_{m,n}} \qquad (9)$$

$$e^{j+1}_{m,n} = \frac{\{[\rho(e+q)]^j_{m,n} - (\rho q)^{j+1}_{m,n} + \frac{\Delta t}{r_m} F_4(\bar{\rho}^{j+1}, \bar{u}^{j+1}, \bar{v}^{j+1}, \bar{e}^{j+1}, \bar{u}^{j+1}, \bar{k}^{j+1}, \bar{\zeta}^{j+1}, \bar{\nu}^{j+1}, \bar{u}^{j+1}, \bar{v}^{j+1})_{m,n}\}}{\rho^{j+1}_{m,n} + \frac{\gamma_\infty}{P_r Re_\infty} \frac{\Delta t}{r_m} G_4 (\bar{k}^{j+1})_{m,n}}$$

where

$$F_1(\rho^j, u^j, v^j)_{m,n} =$$

$$- \frac{1}{(\alpha+1)\Delta x} [(\rho r u)^j_{m,n+1} - (\rho r u)^j_{m,n-1}]$$

$$- \frac{1}{(\beta+1)\Delta r} [(\rho r v)^j_{m+1,n} - (\rho r v)^j_{m-1,n}]$$

$$F_2(\rho^j, u^j, v^j, e^j, u^j, X^j)_{m,n} =$$

$$- \frac{1}{(\alpha+1)\Delta x} \left\{ [\rho r (u^2 + \hat{M}_\infty eX)]^j_{m,n+1} - [\rho r (u^2 + \hat{M}_\infty eX)]^j_{m,n-1} \right\}$$

$$- \frac{1}{(\beta+1)\Delta r} [(\rho r u v)^j_{m+1,n} - (\rho r u v)^j_{m-1,n}]$$

(10)

$$+ \frac{1}{Re_\infty} \left\{ \frac{4/3}{\alpha(\alpha+1)\Delta x^2} \left[[(r\mu)^j_{m,n+1} + (r\mu)^j_{m,n}] u^j_{m,n+1} + \alpha[(r\mu)^j_{m,n} + (r\mu)^j_{m,n-1}] u^j_{m,n-1} \right] \right.$$

$$\left. + \frac{1}{\beta(\beta+1)\Delta r^2} \left[[(r\mu)^j_{m+1,n} + (r\mu)^j_{m,n}] u^j_{m+1,n} + \beta[(r\mu)^j_{m,n} + (r\mu)^j_{m-1,n}] u^j_{m-1,n} \right] \right.$$

$$- \frac{2/3}{(\alpha+1)(\beta+1)\Delta x \Delta r}\left[(r\mu)^j_{m,n+1}\left(v^j_{m+1,n+1} - v^j_{m-1,n+1}\right)\right.$$

$$\left. - (r\mu)^j_{m,n-1}\left(v^j_{m+1,n-1} - v^j_{m-1,n-1}\right)\right]$$

$$+ \frac{1}{(\alpha+1)(\beta+1)\Delta x \Delta r}\left[(r\mu)^j_{m+1,n}\left(v^j_{m+1,n+1} - v^j_{m+1,n-1}\right)\right.$$

$$\left. - (r\mu)^j_{m-1,n}\left(v^j_{m-1,n+1} - v^j_{m-1,n-1}\right)\right]$$

$$\left. - \frac{2/3}{(\alpha+1)\Delta x}\left[(\mu v)^j_{m,n+1} - (\mu v)^j_{m,n-1}\right]\right\}$$

$$F_3\left(\rho^j, u^j, v^j, e^j, \mu^j, X^j\right)_{m,n} =$$

$$- \frac{1}{(\beta+1)\Delta r}\left\{\left[\rho r\left(v^2 + \hat{M}_\infty eX\right)\right]^j_{m+1,n} - \left[\rho r\left(v^2 + \hat{M}_\infty eX\right)^j_{m-1,n}\right]\right\}$$

$$- \frac{1}{(\alpha+1)\Delta x}\left[(\rho ruv)^j_{m,n+1} - (\rho ruv)^j_{m,n-1}\right]$$

$$+ \frac{1}{Re_\infty}\left\{\frac{4/3}{\beta(\beta+1)\Delta r^2}\left[\left[r\mu\right)^j_{m+1,n} + (r\mu)^j_{m,n}\right] v^j_{m+1,n}\right.$$

$$\left. + \beta\left[(r\mu)^j_{m,n} + (r\mu)^j_{m-1,n}\right] v^j_{m-1,n}\right]$$

$$+ \frac{1}{\alpha(\alpha+1)\Delta x^2}\left[\left[(r\mu)^j_{m,n+1} + (r\mu)^j_{m,n}\right] v^j_{m,n+1}\right.$$

$$\left. + \alpha\left[(r\mu)^j_{m,n} + (r\mu)^j_{m,n-1}\right] v^j_{m,n-1}\right]$$

(10 cont

$$- \frac{2/3}{(\alpha+1)(\beta+1)\Delta x \Delta r} \left[(r\mu)^j_{m+1,n} \left(u^j_{m+1,n+1} - u^j_{m+1,n-1}\right) \right.$$

$$\left. - (r\mu)^j_{m-1,n} \left(u^j_{m-1,n+1} - u^j_{m-1,n-1}\right) \right]$$

$$+ \frac{1}{(\alpha+1)(\beta+1)\Delta x \Delta r} \left[(r\mu)^j_{m,n+1} \left(u^j_{m+1,n+1} - u^j_{m-1,n+1}\right) \right.$$

$$\left. - (r\mu)^j_{m,n-1} \left(u^j_{m+1,n-1} - u^j_{m-1,n-1}\right) \right]$$

$$- \frac{2/3}{(\beta+1)\Delta r} \left[(\mu v)^j_{m+1,n} - (\mu v)^j_{m-1,n} \right]$$

$$+ \frac{(2/3)\mu^j_{m,n}}{(\beta+1)\Delta r} \left(v^j_{m+1,n} - v^j_{m-1,n}\right)$$

$$+ \frac{(2/3)\mu^j_{m,n}}{(\alpha+1)\Delta x} \left(u^j_{m,n+1} - u^j_{m,n-1}\right)$$

$$\left. - \frac{4}{3} \frac{(\mu v)^j_{m,n}}{r_m} \right\} + \left(\rho \hat{M}_\infty eX\right)^j_{m,n} \qquad \text{(10 cont'd)}$$

$$F_4\left(\rho^j, u^j, v^j, e^j, \mu^j, k^j, \zeta^j, \gamma^j, \bar{u}^{j+1}, \bar{v}^{j+1}\right)_{m,n} =$$

$$- \frac{1}{(\alpha+1)\Delta x} \left\{ \left[\rho ru(\gamma e+q)\right]^j_{m,n+1} - \left[\rho ru(\gamma e+q)\right]^j_{m,n-1} \right\}$$

$$- \frac{1}{(\beta+1)\Delta r} \left\{ \left[\rho rv(\gamma e+q)\right]^j_{m+1,n} - \left[\rho rv(\gamma e+q)\right]^j_{m-1,n} \right\}$$

$$+\frac{\gamma_\infty}{P_r\,Re_\infty}\left\{\frac{1}{\alpha(\alpha+1)\Delta x^2}\left[(rk)^j_{m,n+1}+(rk)^j_{m,n}\right](\zeta e)^j_{m,n+1}\right.$$

$$\left.+\alpha\left[(rk)^j_{m,n}+(rk)^j_{m,n-1}\right](\zeta e)^j_{m,n-1}\right]$$

$$+\frac{1}{\beta(\beta+1)\Delta r^2}\left\{\left[(rk)^j_{m+1,n}+(rk)^j_{m,n}\right](\zeta e)^j_{m+1,n}\right.$$

$$\left.+\beta\left[(rk)^j_{m,n}+(rk)^j_{m-1,n}\right](\zeta e)^j_{m-1,n}\right\}$$

$$+\frac{\bar{M}_\infty}{Re_\infty}\left\{\frac{2/3}{\alpha(\alpha+1)\Delta x^2}\left[(r\mu)^j_{m,n+1}+(r\mu)^j_{m,n}\right](u^j_{m,n+1})^2\right.$$

$$-\left[(r\mu)^j_{m,n+1}+(1+\alpha)(r\mu)^j_{m,n}+\alpha(r\mu)^j_{m,n-1}\right](u^{j+1}_{m,n})^2$$

$$\left.+\alpha\left[(r\mu)^j_{m,n}+(r\mu)^j_{m,n-1}\right](u^j_{m,n-1})^2\right]$$

$$+\frac{1/2}{\alpha(\alpha+1)\Delta x^2}\left[(r\mu)^j_{m,n+1}+(r\mu)^j_{m,n}\right](v^j_{m,n+1})^2 \qquad \text{(10 cont'}$$

$$-\left[(r\mu)^j_{m,n+1}+(1+\alpha)(r\mu)^j_{m,n}+\alpha(r\mu)^j_{m,n-1}\right](\bar{v}^{j+1}_{m,n})^2$$

$$\left.+\alpha\left[(r\mu)^j_{m,n}+(r\mu)^j_{m,n-1}\right](v^j_{m,n-1})^2\right]$$

$$-\frac{2/3}{(\alpha+1)(\beta+1)\Delta x\Delta r}\left[(r\mu u)^j_{m,n+1}\,(v^j_{m+1,n+1}-v^j_{m-1,n+1})\right.$$

$$\left.-(r\mu u)^j_{m,n-1}\,(v^j_{m+1,n-1}-v^j_{m-1,n-1})\right]$$

$$+\frac{1}{(\alpha+1)(\beta+1)\Delta x\Delta r}\left[(r\mu v)^j_{m,n+1}\,(u^j_{m+1,n+1}-u^j_{m-1,n+1})\right.$$

$$\left.-(r\mu v)^j_{m,n-1}\,(u^j_{m+1,n-1}-u^j_{m-1,n-1})\right]$$

$$- \frac{2/3}{(\alpha+1)\Delta x} \left[(\mu u v)^j_{m,n+1} - (\mu u v)^j_{m,n-1} \right]$$

$$+ \frac{2/3}{\beta(\beta+1)\Delta r} \Big\{ \left[(r\mu)^j_{m+1,n} + (r\mu)^j_{m-1,n} \right] (v^j_{m+1,n})^2$$

$$- \left[(r\mu)^j_{m+1,n} + (1+\beta)(r\mu)^j_{m,n} + \beta (r\mu)^j_{m-1,n} \right] (\bar{v}^{j+1}_{m,n})^2$$

$$+ \beta \left[(r\mu)^j_{m,n} + (r\mu)^j_{m-1,n} \right] (v^j_{m-1,n})^2 \Big\}$$

$$+ \frac{1/2}{\beta(\beta+1)\Delta r^2} \Big\{ \left[(r\mu)^j_{m+1,n} + (r\mu)^j_{m,n} \right] (u^j_{m+1,n})^2$$

$$- \left[(r\mu)^j_{m+1,n} + (1+\beta)(r\mu)^j_{m,n} + \beta (r\mu)^j_{m-1,n} \right] (\bar{u}^{j+1}_{m,n})^2$$

$$+ \beta \left[(r\mu)^j_{m,n} + (r\mu)^j_{m-1,n} \right] (u^j_{m-1,n})^2 \Big\} \qquad \text{(10 concld)}$$

$$- \frac{2/3}{(\alpha+1)(\beta+1)\Delta x \Delta r} \left[(r\mu v)^j_{m+1,n} \left(u^j_{m+1,n+1} - u^j_{m+1,n-1} \right) \right.$$

$$\left. - (r\mu v)^j_{m-1,n} \left(u^j_{m-1,n+1} - u^j_{m-1,n-1} \right) \right]$$

$$+ \frac{1}{(\alpha+1)(\beta+1)\Delta x \Delta r} \left[(r\mu u)^j_{m+1,n} \left(v^j_{m+1,n+1} - v^j_{m+1,n-1} \right) \right.$$

$$\left. - (r\mu u)^j_{m-1,n} \left(v^j_{m-1,n+1} - v^j_{m-1,n-1} \right) \right]$$

$$- \frac{2/3}{(\beta+1)\Delta r} \left[(\mu v^2)^j_{m+1,n} - (\mu v)^j_{m-1,n} \right] \Big\}$$

and

$$G_2(\mu^j)_{m,n} =$$

$$\frac{4/3}{\alpha(\alpha+1)\Delta x^2} \left[(r\mu)^j_{m,n+1} + (1+\alpha)(r\mu)^j_{m,n} + \alpha (r\mu)^j_{m,n-1} \right] \qquad (11)$$

$$+ \frac{1}{\beta(\beta+1)\Delta r^2}\left[(r\mu)^j_{m+1,n} + (1+\beta)(r\mu)^j_{m,n} + \beta\,(r\mu)^j_{m-1,n}\right]$$

$$G_3(\mu^j)_{m,n} =$$

$$\frac{4/3}{\beta(\beta+1)\Delta r^2}\left[(r\mu)^j_{m+1,n} + (1+\beta)(r\mu)^j_{m,n} + \beta(r\mu)^j_{m-1,n}\right]$$

$$+ \frac{1}{\alpha(\alpha+1)\Delta x^2}\left[(r\mu)^j_{m,n+1} + (1+\alpha)(r\mu)^j_{m,n} + \alpha(r\mu)^j_{m,n-1}\right]$$

$$G_4(k^j)_{m,n} =$$

$$\frac{1}{\alpha(\alpha+1)\Delta x^2}\left[(rk)^j_{m,n+1} + (1+\alpha)(rk)^j_{m,n} + \alpha(rk)^j_{m,n-1}\right]$$

(11 concld)

$$+ \frac{1}{\beta(\beta+1)\Delta r^2}\left[(rk)^j_{m+1,n} + (1+\beta)(rk)^j_{m,n} + \beta(rk)^j_{m-1,n}\right]$$

The normalized viscosities, μ, are obtained from $e_{m,n}$ through Sutherland's law

$$\mu_{m,n} = (e_{m,n})^{3/2}\,(1+a)/(e_{m,n}+a)$$

where a is a constant and the normalized thermal conductivity, k, from the definition of Pr (for a perfect gas $k = \mu$).

Note that the same functions F and G are used in both steps of the iteration procedure and the same mesh is used for both steps. As pointed out by Cheng[3] and Allen,[4,5] this simplifies the program considerably.

In the actual computer programming of these difference equations the F functions are broken into the sum of two functions, $\bar{F}$ and H. The $\bar{F}$ terms contain the non-central portions of the twice spatially differenced diffusive terms whose central portions have been used at the updated time level. These updated central terms have been transposed, combined with the left hand side and divided through, appearing as the G functions. The $\bar{F}_4$ function, which is part of the energy equation, is somewhat special in that it also contains some complete differenced velocity terms in which the central terms are at the updated time level. These updated velocities are known from the solution of the momentum equations.

The H functions contain all of the terms which are not twice differenced diffusive in nature and therefore have no portions at the updated time level. These terms are calculated by general differencing subroutines, which use difference forms given by Eqs. (2), (6) and (7) at time level j.

This break up of the F functions removes the requirement of writing out and programming the difference form of the complete set of differential equations. Only the $\bar{F}$ and G functions need be written out explicitly while the H terms are calculated from the general subroutines.

The requirement used to check the approach of the unsteady calculation to the steady state is that the density change between two successive time steps at the grid point of maximum change should be less than a prescribed small number.

$$\max_{m,n} \left| \rho^{j+1} - \rho^{j} \right| < \epsilon \qquad (12)$$

BOUNDARIES

The preceding set of difference equations is used to compute the flow field in the interior of the domain ABCFGHJA of Figure 1. It remains to develop procedures for treating the six boundaries of this domain.

Upstream

As noted earler, the flow field along the upstream boundary ABC is known from a patching of an inviscid characteristics solution and a boundary layer solution.[6] The values of the independent variables; ρ, u, v, e, from these solutions are used as fixed (with time) upstream boundary conditions alcng line AC.

Body Wall and Base

The body wall and base boundaries, AJ and JH respectively, can be made equivalent to each other by interchanging x and r. In accordance with Allen's numerical results of negative densities on the body,[4] mesh points on the body base and wall are being avoided and these boundaries are taken at mid-mesh locations as shown below for the body wall.

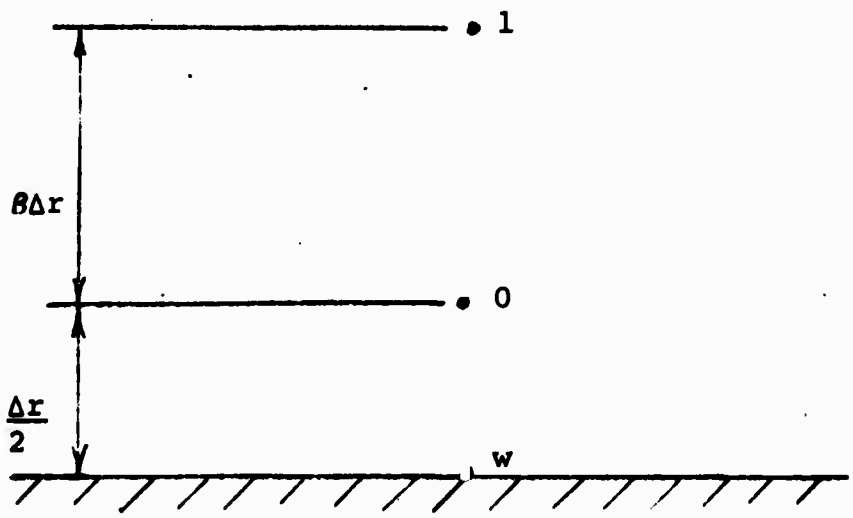

Allen's emphasis on the preservation of conservation in the difference formulation of boundary conditions is being observed; however, our approach to this differs from his (which appears to break down for a nonuniform mesh). We accomplish conservation through an inverse consideration of telescoping of terms under quadrature approximation to integration. That is, we form the boundary conditions so that telescoping of internal contributions and proper appearance of wall terms occurs under quadrature. This procedure should automatically insure the global conservation of mass, momentum and energy.

An open ended trapezoidal integration of the difference form is carried out between the wall and the outer boundary, i.e., for the first radial difference:

$$\int_{r_w}^{r_\infty} f_r dr = f_\infty - f_w = f_r|_o \left(\frac{\Delta r + \beta \Delta r}{2}\right) + f_r|_1 \left(\frac{\beta \Delta r + \delta \Delta r}{2}\right) + \ldots \tag{13}$$

Point 1 and those above it are general points, so a general radial first difference form similar to Eq. (2) is used for $f_r|_1$, $f_r|_2$ etc. Then satisfaction of the telescoping requirement near the wall in Eq. (13) leads to a three point first difference form at point o

$$f_r|_{o,n} = \frac{f_{1,n} + f_{o,n} - 2f_{w,n}}{(1+\beta)\Delta r} \tag{14}$$

Actually, this procedure will also yield a special difference form for $f_r|_\infty$, but it will never be used since no difference equations are applied at the outer boundary. This same procedure can be used for the second derivatives and cross derivatives.

$$(af_r)_r|_{o,n} = \Big\{[(1+2\beta)(a_{o,n}+a_{1,n}) + 2a_{w,n}]\, f_{1,n}$$

$$- (1+2\beta)[a_{o,n}+a_{1,n} + 2(1+2\beta)\, a_{w,n}]\, f_{o,n}$$

$$+ 8\beta(\beta+1)\, a_{w,n}\, f_{w,n} \Big\} \,/\, \beta(1+\beta)(1+2\beta)\, \Delta r^2 \tag{15}$$

$$(af_x)_r|_{o,n} = [a_{1,n}(f_{1,n+1}-f_{1,n-1}) + a_{o,n}(f_{o,n+1}-f_{o,n-1})$$

$$- 2\, a_{w,n}(f_{w,n+1}-f_{w,n-1})]/(1+\alpha)(1+\beta)\, \Delta x \Delta r \tag{16}$$

$$(af_r)_x|_{o,n} = [a_{o,n+1}(f_{o,n+1}+f_{1,n+1} - 2\, f_{w,n+1})$$

$$- a_{o,n-1}(f_{o,n-1}+f_{1,n-1} - 2\, f_{w,n-1})]/(1+\alpha)(1+\beta)\, \Delta x \Delta r \tag{17}$$

A possibly more accurate scheme can be obtained by using closed ended integration

$$\int_{r_w}^{r_\infty} f_r dr = f_\infty - f_w = f_r|_w \frac{\Delta r}{4} + f_r|_o \left(\frac{\Delta r}{4} + \frac{\beta \Delta r}{2}\right)$$

$$+ f_r|_1 \left(\frac{\beta \Delta r + \delta \Delta r}{2}\right) + \ldots \tag{18}$$

Point 1 and those above it are still general. However, a second order accurate difference formula can be used at point o

$$f_r|_{o,n} = \frac{-4\beta^2\, f_{w,n} + (4\beta^2-1)\, f_{o,n} + f_{1,n}}{\beta(2\beta+1)\, \Delta r} \tag{19}$$

and conservation form can still be retained by solving for the $f_r|_w$ which satisffes Eq. (18).

$$f_r|_{w,n} = \frac{-[4\beta(1-\beta)\ f_{w,n} + (4\beta^2-2\beta-1) f_{o,n}]}{\beta \Delta r}$$

This backed out difference form at the wall is never actually used since no difference equations are used along the wall but a half mesh out. The difference forms obtained from this closed integration scheme were programmed but no calculations were carried out. All of the results discussed later use the open ended integration difference forms given by Eq. (14) - (17). For reference, the second and cross difference forms for the closed integration scheme are presented here, even though they have not yet been used in the numerical examples.

$$(af_r)_r|_{o,n} = \{[(4\beta-1)\ a_{o,n} + a_{1,n}]\ f_{1,n}$$

$$+ [(1+2\beta)(4\beta^2-6\beta+1)\ a_{o,n} - a_{1,n} - 8\beta^3 a_{w,n}]\ f_{o,n}$$

$$+ 8\beta^2[(1-\beta)\ a_{o,n} + \beta a_{w,n}]\ f_{w,n}\} \ /\ \beta^2(1+2\beta)\ \Delta r^2$$

$$(af_r)_x|_{o,n} = \{a_{o,n+1}[-4\beta^2 f_{w,n+1} + (4\beta^2-1)\ f_{o,n+1} + f_{1,n+1}]$$

$$- a_{o,n-1}[-4\beta^2\ f_{w,n-1} + (4\beta^2-1)\ f_{o,n-1} + f_{1,n-1}]/\beta(1+\alpha)(1+2\beta)\Delta x \Delta r$$

$$(af_x)_r\big|_{o,n} = \Big\{-4\beta^2 a_{w,n}(f_{w,n+1}-f_{w,n-1}) + (4\beta^2-1)\, a_{o,n}(f_{o,n+1}-f_{o,n-1})$$

$$+ a_{1,n}(f_{1,n+1}-f_{1,n-1})\Big\} \;/\; R(1+\alpha)(1+2\beta)\,\Delta x \Delta r \;.$$

Since the finite difference equations are not applied along the wall it is necessary to obtain wall values by other means. The velocity components u and v are both known to be zero on the body wall and base. For other quantities such as ρ, $r\mu$, rk, X and ζ, a two point extrapolation is used

$$f_{w,n} = [(1+2\beta)\, f_{o,n} - f_{1,n}]/2\beta \qquad (20)$$

The wall density need only be computed at the final time if the products $(\rho u)_{w,n}$ and $(\rho v)_{w,n}$ are recognized as being zero.

Either of two wall boundary conditions are employed to obtain $e_{w,n}$. A constant wall temperature condition can be appl[illegible] by simply setting

$$e_{w,n} = \text{constant} \qquad (21)$$

It appears that it would be possible for this constant to vary along the wall, but this was not attempted here for the sake of simplicity. For an adiabatic wall the condition that $\partial e/\partial r = 0$ can be satisfied by requiring

$$e_{w,n} = e_{o,n} \qquad (22)$$

Both of these options are provided in the computer program.

The general point time difference scheme, namely Eqs.(8) and (9) can still be used for points one half mesh from the body. The F functions are broken up into $\bar{F}$ and H functions as described before. The H functions remain the same as the general case except that Eqs.(14) to (17) are used to compute all radial differences. The $\bar{F}$ and G functions for points one half mesh from the body surface are given for reference in Appendix I. The quantities $(r\mu)_{w,n}$, $(rk)_{w,n}$ and $\zeta_{w,n}$ are obtained from the extrapolation formula (20) at each time step. The difference equations along a line of grid points one half a mesh behind the body base can be similarly obtained or can be evolved from the body wall equations by interchanging x and r, α and β, and u and v.

There are three points at the corner formed by the body wall and base, which require special considerations. These points are designated in Figure 2 as m, n-1; m,n and m-1,n. They are special because mixed derivatives require difference forms of both side wall and base wall types. Judicious use of the individual difference forms results in the following results for the mixed derivative differences at these points.

$$(af_r)_x|_{m,n-1} = \{a_{m,n}(f_{m+1,n}-f_{m-1,n}) - [(1+\beta)/\beta]a_{m,n-2}(f_{m+1,n-2}-f_{m,n-2})\}/(1+\alpha)(1+\beta)\Delta x\Delta r \qquad (23a)$$

$$(af_x)_r|_{m,n-1}=[a_{m+1,n-1}(f_{m+1,n}-f_{m+1,n-2})$$

$$-a_{m,n-1}(f_{m,n}-f_{m,n-2})]/(1+\alpha)\beta\ \Delta x\Delta r \tag{23b}$$

$$(af_r)_x|_{m,n}=\{a_{m,n+1}(f_{m+1,n+1}-f_{m-1,n+1})$$

$$-[(1+\beta)/\beta]\ a_{m,n-1}(f_{m+1,n-1}-f_{m,n-1})\}/(1+\alpha)(1+\beta)\ \Delta x\Delta r \tag{23c}$$

$$(af_x)_r|_{m,n}=\{a_{m+1,n}(f_{m+1,n+1}-f_{m+1,n-1})$$

$$+[(1+\alpha)/\alpha]\ a_{m-1,n}\ (f_{m-1,n+1}-f_{m-1,n})\}/(1+\alpha)(1+\beta)\ \Delta x\Delta r \tag{23d}$$

$$(af_r)_x|_{m-1,n}=[a_{m-1,n+1}(f_{m,n+1}-f_{m-2,n+1})$$

$$-a_{m-1,n}(f_{m,n}-f_{m-2,n})]/\alpha(1+\beta)\ \Delta x\Delta r \tag{23e}$$

$$(af_x)_r|_{m-1,n}=\{a_{m,n}(f_{m,n+1}-f_{m,n-1})$$

$$-[(1+\alpha)/\alpha]\ a_{m-2,n}(f_{m-2,n+1}-f_{m-2,n})\}/(1+\alpha)(1+\beta)\Delta x\Delta r \tag{23f}$$

These derivatives only appear in the H functions, therefore the appropriate $\bar{F}$ and G functions can be used at each point with special subroutines for the mixed derivatives in the H functions only.

Centerline

Along the boundary represented by the axis of symmetry in the wake, mesh points are again avoided. A special finite difference equation for use one mesh away from the axis has been developed using an inverse telescoping procedure similar to that used for the wall boundaries. This case is more complex since the radial difference schemes depend on whether the function being differenced is odd or even with respect to radius near the axis. The two odd variables are r and v, while the other variables ρ, u, e, μ, etc. are even. Combinations of these variables are considered even if they contain none or an even number of odd variables and are considered odd if they contain an odd number of odd variables.

By definition, an even function has zero first derivative at the axis, r = 0. Therefore, if an open ended integration of the first difference similar to Eq. (13) is carried out between the center line and the outer boundary

$$\int_0^{r_\infty} f_r dr = f_\infty - f_c = f_r|_1 \frac{(\Delta r + \beta \Delta r)}{2} + f_r|_2 \left(\frac{\beta \Delta r + \delta \Delta r}{2}\right) + \ldots \tag{24}$$

and the general first radial difference form, equivalent to Eq. (2), is used for points 2 and above, the satisfaction of the telescoping

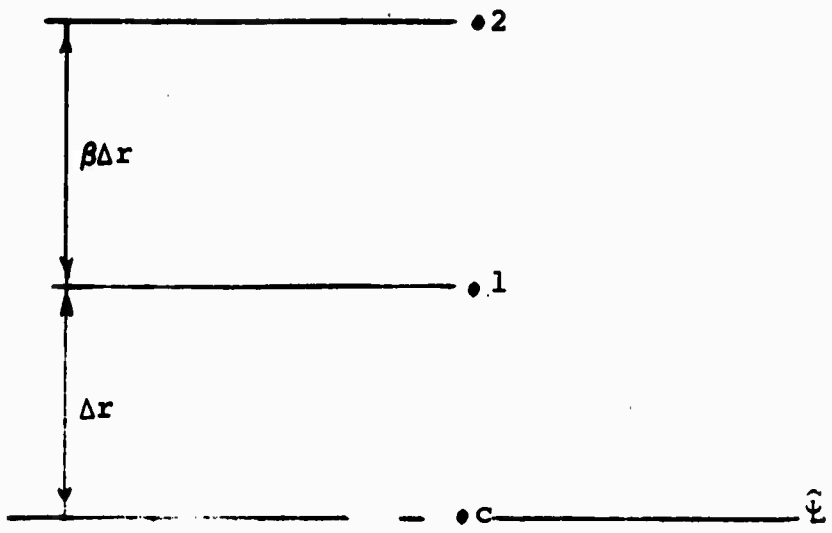

requirement in Eq. (24) yields a special first difference form for point 1.

$$f_r|_{1,n} = (f_{1,n}+f_{2,n}-2f_{c,n})/(1+\beta)\ \Delta r \qquad \text{(f even)} \qquad (25)$$

For an odd function $f_c = 0$ instead of $f_r|_c$. Then the general form can be used at point 1 and a special form for $f_r|_c$ determined by the telescoping requirement. However, since no difference equations are used at the center line this special difference form is never used. Since $f_c = 0$, the first difference form at point 1 reduces to

$$f_r|_{1,n} = f_{2,n}/(1+\beta)\ \Delta r \qquad \text{(f odd)} \qquad (26)$$

For an even function the value of the function on the center line, f_c, is required. For this scheme f_c is obtained by a two point extrapolation

$$f_{c,n} = [f_{1,n}(1+\beta)^2 - f_{2,n}]/\beta(\beta+2) \qquad \text{(f even)} \qquad (27)$$

The higher order differences can be obtained in a similar manner. Inspection of the differential equations shows that all coefficients a in derivatives of the form $(a\ f_r)_r$ are odd. Using $a_c=0$, the telescoping requirement yields the second difference forms

$$(af_r)_r|_{1,n} = (a_1+a_2)(f_2-f_1)/\beta(\beta+1)\ \Delta r^2 \qquad \text{(f even)} \tag{28}$$

$$(af_r)_r|_{1,n} = \left\{(a_1+a_2)f_2-[(1+\beta)a_1+a_2]f_1\right\}/\beta(\beta+1)\Delta r^2 \qquad \text{(f odd)} \tag{29}$$

Eq. (29) is the general form with $f_c = 0$.

The cross derivative difference forms are obtained similarly, exercising care as to the odd or even nature of the coefficients a.

$$(af_r)_x|_{1,n} = [a_{1,n+1}(f_{1,n+1}+f_{2,n+1}-2\ f_{c,n+1}) - a_{1,n-1}(f_{1,n-1}+f_{2,n-1}-2\ f_{c,n-1})]/(1+\alpha)(1+\beta)\ \Delta x\Delta r \qquad \text{(f even)} \tag{30}$$

$$(af_r)_x|_{1,n} = [a_{1,n+1}f_{2,n+1}-a_{1,n-1}f_{2,n-1}]/(1+\alpha)(1+\beta)\ \Delta x\Delta r \qquad \text{(f odd)} \tag{31}$$

$$(af_x)_r|_{1,n} = [a_{1,n}(f_{1,n+1}-f_{1,n-1}) + a_{2,n}(f_{2,n+1}-f_{2,n-1}) \quad \begin{Bmatrix}\text{a even, f even}\\ \text{a odd, or f odd}\end{Bmatrix} - 2a_{c,n}(f_{c,n+1}-f_{c,n-1})]/(1+\alpha)(1+\beta)\ \Delta x\Delta r \tag{32}$$

$$(af_x)_r|_{1,n} = a_{2,n}(f_{2,n+1}-f_{2,n-1})/(1+\alpha(1+\beta)\ \Delta x\Delta r \qquad \left\{\begin{matrix}a \text{ even}, & \text{or} & f \text{ odd} \\ a \text{ odd}, & & f \text{ even}\end{matrix}\right\} \tag{33}$$

Eqs. (25) to (33) represent the difference scheme actually programmed for points one mesh off the wake center line. However, the numerical solution showed kinks near the axes in the radial density plot. The extrapolation for center line values of even functions was judged the cause of these kinks and a new center line differencing scheme was developed but is not incorporated into the computer program from which numerical results were obtained. The change concerns the even functions, which have $f_{r_c} = 0$. Instead of finding f_{r_1} by telescoping and extrapolating for f_c, the general difference form can be used for f_{r_1} and the telescoping requirement on Eq. (24) used to find f_c. This results in

$$f_c = f_1 \qquad (f \text{ even}) \tag{34}$$

and eliminates the need for extrapolations. The first difference form is then

$$f_r|_{1,n} = (f_{2,n}-f_{1,n})/(1+\beta)\ \Delta r \qquad (f \text{ even}) \tag{35}$$

The second difference forms are unchanged and the cross-derivatives which are changed are

$$(af_r)_x|_{1,n} = [a_{1,n+1}(f_{2,n+1}-f_{1,n+1}) \qquad (f \text{ even})$$
$$- a_{1,n-1}(f_{2,n-1}-f_{1,n-1})]/(1+\alpha)(1+\beta)\ \Delta x\Delta r \tag{36}$$

$$(af_x)_r|_{1,n} = [a_{2,n}(f_{2,n+1}-f_{2,n-1}) \qquad \begin{Bmatrix} a \text{ even}, & f \text{ odd} \\ a \text{ odd}, & f \text{ even} \end{Bmatrix}$$

$$- a_{c,n}(f_{1,n+1}-f_{1,n-1})]/(1+\alpha)(1+\beta)\ \Delta x \Delta r \qquad (37)$$

At the final time step Eq. (27) can be used to obtain center line values of the even functions. The $\bar{F}$ and G functions resulting from using these difference forms in the differential equations are identical for either scheme and only the subroutines for computing the H functions are affected.

It should also be noted that a completely different center line differencing scheme can be obtained by use of closed ended integration in the telescoping condition. Most of these improvements were programmed in preparation for a trial of a turbulent base flow calculation (see Appendix III) but no actual calculations were carried out.

The $\bar{F}$ and G functions for points one mesh above the axis which are used in the general iteration scheme, are given in Appendix I. The H functions are the same as a general point with Eqs. (25) to (33) supplying the special difference subroutines for the center line.

Special difference formulas are needed at point 1, 0 (see Figure 3), since it is adjacent to both the base wall and the wake center line. The first and second differences are the same as those along the boundaries they include. The axial (x) derivatives are the same as those one half mesh from the base wall, i.e., the axial forms of Eqs. (14) and (15), while the radial derivatives are the same as the center line forms, Eqs. (25)-(27). The mixed derivatives are obtained by successive applications of the respective first

differences. These are listed below for reference:

$$(af_r)_x|_{1,o} = \{a_{1,o}(f_{1,o}+f_{2,o}-2f_{c,o}) + a_{1,1}(f_{1,1}+f_{2,1}-2f_{c,1}) - 2a_{1,w}(f_{1,w}+f_{2,w}-2f_{c,w})\}/(1+\alpha)(1+\beta)\,\Delta x\Delta r \qquad \text{(f even)} \qquad (38)$$

$$(af_r)_x|_{1,o} = \{a_{1,o}f_{2,o}+a_{1,1}f_{2,1}-2\,a_{1,w}f_{2,w}\}/(1+\alpha)(1+\beta)\,\Delta x\Delta r \qquad \text{(f odd)} \qquad (39)$$

$$(af_x)_r|_{1,o} = \{a_{1,o}(f_{1,o}+f_{1,1}-2f_{1,w}) + a_{2,o}(f_{2,o}+f_{2,1}-2f_{2,w}) \quad \begin{cases} a \text{ even, } f \text{ even} \\ a \text{ odd, or } f \text{ odd} \end{cases} - 2a_{c,o}(f_{c,o}+f_{c,1}-2f_{c,w})\}/(1+\alpha)(1+\beta)\,\Delta x\Delta r \qquad (40)$$

$$(af_x)_r|_{1,o} = a_{2,o}(f_{2,o}+f_{2,1}-2f_{2,w})/(1+\alpha)(1+\beta)\,\Delta x\Delta r \qquad \text{(a odd, f even)} \qquad (41)$$

Values of functions at point c, o are obtained by the normal center line extrapolation formula, Eq. (27), while functions at point 1, w are obtained by extrapolation from the axial form of Eq. (20). All the functions required at point c, w contain $u_{c,w}$ or $v_{c,w}$ which are zero making extrapolation unnecessary.

However, it would be of interest to have values for $\rho_{c,w}$ and $e_{c,w}$ for the final steady state solution. Except for the constant wall temperature case where $e_{c,w} = e_w$, these variables have been left undetermined due to the ambiguity of the extrapolation procedures.

The general forms of the H functions are used with the appropriate difference forms. This special point requires its own set of $\bar{F}$ and G functions for use in the general iteration scheme. These are listed in Appendix I.

Downstream

The downstream boundary conditions have been formulated in a three-point, variable mesh extrapolation along lines of constant radius. Allen[4] found this procedure to be satisfactory if the boundary is chosen far enough downstream for the flow to have returned to almost completely supersonic speeds (for use of the downstream data line as input to a far wake program the flow must be completely supersonic). Another restriction is that the angle between the streamline and the constant radius line at each downstream boundary point must be less than the local Mach angle. Otherwise the upstream points on the constant radius line will not lie in the zone of influence of the boundary point.

Figure 4 shows the nomenclature for the downstream extrapolation. The second order accurate, three point, variable mesh extrapolation formula for point m,N is

$$f_{m,N} = [\Delta x_{N-2}(\Delta x_N+\Delta x_{N-1})(\Delta x_N+\Delta x_{N-1}+\Delta x_{N-2})\ f_{m,N-1}$$

$$- \Delta x_N(\Delta x_{N-1}+\Delta x_{N-2})(\Delta x_N+\Delta x_{N-1}+\Delta x_{N-2})\ f_{m,N-2}$$

$$+ \Delta x_N\Delta x_{N-1}(\Delta x_N+\Delta x_{N-1})\ f_{m,N-3}]/\Delta x_{N-1}\Delta x_{N-2}(\Delta x_{N-1}+\Delta x_{N-2}) \qquad (42)$$

This relation can be used to obtain the values of each variable at each time step for both parts of the two step iteration.

Upper Boundary

It is desired to obtain values of the independent variables at outer most radial grid (CF in Figure 1) by an extrapolation procedure. The location of this upper boundary line is picked in such a way that the flow adjacent to it is inviscid and supersonic. The downstream boundary, EG, is picked where the center line flow is expected to be supersonic. Then the first family characteristic line, BF, is constructed from point B, which is in the supersonic, inviscid region of the upstream data line above the boundary layer. Point F is determined by the intersection of this line and the downstream boundary line EG. Then line CF will lie completely above characteristic line BF and the flow adjacent to it will be inviscid since the viscous effects generated in the boundary layer portion of the inflow, AB, cannot propagate across the characteristic line.

Allen[4] used an extrapolation procedure which involves an inviscid, steady state simple wave characteristic solution. The present problem requires a more complex procedure due to the axisymmetry and the nonuniform flow external to CF, which is obtained from an independent inviscid flow field calculation. The current method involves a steady state, two step characteristics extrapolation. The use of a steady state solution means the numerical results will be incorrect during their time evolution, but when a steady state is reached, it will be correct.

Figure 5 shows typical grid points near the upper boundary. The line designated by M represents line CF in Figure 1. All points up to line M-1 are computed by the internal difference equations and it is desired to extrapolate this solution to a typical point M,n.

Before describing the technique, some consideration should be given as to just how much data at M,n should be prescribed from the known inviscid solution and how much extrapolated from the interior. For the situation of Figure 5,data are transmitted out of the calculation region at B along two lines; the streamline and the first family characteristic line, while the second family line at B transmits data into the region. Each of the characteristics carries one piece of data, via the characteristic equation, while the streamline carries two pieces via the isentropic and constant stagnation enthalpy conditions. Therefore, for this case one piece of data is prescribed from the external flow, namely the flow deflection θ, and three variables are extrapolated. The numerical examples considered later coincide with this geometry. If a problem with a different characteristics-streamline arrangement were considered the computer program would require modification.

The characteristics iteration is started by knowing from the interior calculations, all the variables along the line of constant radius represented by M-1 and inputing the flow deflection, θ, at each point along the M line. Then for the first iteration step the first family characteristic can be constructed from A to intercept the M line at B (see Reference 9). The x location of point B can be found from

$$x_B = x_A + (r_M - r_{M-1})/\tan(\theta_A + \mu_A) \tag{43}$$

where

$$\theta_A = \tan^{-1}(v_A/u_A) \tag{43a}$$

the Mach angle

$$\mu_A = \sin^{-1}(1/M_A) \tag{43b}$$

and the Mach number

$$M_A = [2q_A/\gamma(\gamma-1)\ e_A]^{\frac{1}{2}} \tag{43c}$$

The value of θ_B can be found by interpolating between points M, n and M,n+1.

Next the streamline from B back toward A can be constructed using an average of slopes at A and B. This locates point C.

$$r_C = r_M - (x_B - x_{n-1}) \ (\tan \theta_A + \tan \theta_B)/2 \qquad (44)$$

It is assumed that the variables at point M, n-1 are known from the preceding extrapolation. If n-1 is the upstream boundary they would be prescribed. Then the values of ρ,e and q at C can be found by interpolation between points A and M,n-1.

Two conditions are known to apply along the streamline CB.[9] The first, which requires the flow to be isentropic along the streamline can be expressed by relating the normalized pressure and density as follows

$$P = d \ \rho^{\gamma} \qquad (45a)$$

where d is a constant and the equation of state gives $P = X \ \rho e$. Elimination of P allows Eq. (45a) to be written

$$d = X \ e (\rho)^{1-\gamma} \qquad (45b)$$

The second condition is that the stagnation enthalpy is constant along a streamline

$$H = e + q = \text{constant} \qquad (46)$$

The values of the constants d and H can be evaluated by applying equations (45b) and (46) at point C. These will be used later at point B.

Next the first family characteristic equation[9] along line AB can be used to obtain the normalized pressure at B. For the first iteration step this equation is

$$P_B = P_A - [2\gamma^2 P_A/(\gamma+1)]\{(\theta_B-\theta_A)/\cos\mu_A \sin\mu_A + [\sin\theta_A/r_A \cos\mu_A \cos(\theta_A+\mu_A)](x_B-x_A)\} \quad (47)$$

Since d and H are constant along streamline CB, their values at B are the same as at C so Eqs. (45a), (46) and the state equation can be used at B to determine ρ_B, e_B and q_B from P_B.

$$\rho_B = (P_B/d)^{1/\gamma} \quad (48)$$

$$e_B = P_B/\rho_B X_B \quad (49)$$

$$q_B = H - e_B \quad (50)$$

These quantities together with θ_B represent the first step of the iteration solution at point B. For the second step the process is repeated using average values of the slopes at both ends of the characteristic and stream lines. This more accurately locates points B and C. Equation (47) is recomputed using similarly averaged coefficients of the θ and x terms and final values of ρ_B, e_B, q_B and θ_B are determined. After the second iteration step is completed, the velocities u and v can be obtained from

$$u_B = (2q_B/\bar{M}_\infty)^{\frac{1}{2}} \cos \theta_B$$

$$v_B = (2q_B/\bar{M}_\infty)^{\frac{1}{2}} \sin \theta_B \qquad (51)$$

The values of the four independent variables ρ,u,v and e can be obtained at M,n by interpolating between points M,n-1 and B.

In an actual problem point B may not fall between line n and n+1 but may be between n+1 and n+2 or between n-1 and n, etc. The computer program has taken these possibilities into account by using various interpolations and or extrapolations. The only geometric restriction on the flow is that one characteristic line and the streamline lie below the upper boundary line, while the other characteristic line lies above. The program can be adapted to other cases but this has not been done as yet.

NUMERICAL RESULTS

Computer Program

The finite difference scheme described in the preceding sections was programmed in FORTRAN Version 2.3 (includes all features of FORTRAN IV plus some additions) for the CDC 6400/6500/6600 computers. Three grid configurations were used:

Configuration	1	2	3
r direction grid points	10	50	50
x direction grid points	20	50	70
Total points in mesh	170	2040	3040
Execution time for 2 half-steps on CDC 6600	1.4 sec	15 sec	20.8 sec

The total number of points for any configuration is equal to the product of the numbers of points in the x and r directions minus those points which fall within the body.

It is our estimate that the maximum size grid configuration that could be run (by expanding the appropriate program dimensions) is 90 x 90 or some other combination of x and r grid points whose product is equivalent. This maximum grid size estimate is based upon the program volume, plus the storage necessary for the computer operating system, plus the additional storage needed at load time. The cost of running the expanded grid is approximately predictable from the above table by equating the ratios of execution time and total mesh points. There is another cost factor. The number of iterations to reach convergence is greater with the finer mesh because a disturbance can propagate at most one grid point in one half step.

A separate computer program was written to take data from the intermediate data files (TAPE 7) and create digital plots of velocity vectors, streamlines and pressure contours in the flow field. The plotting was performed on a Calcomp Plotter. The CDC 6600 software required to run this program is the Calcomp Plotter Software package; specifically, subroutines PLØT, SYMBØL and NUMBER. Instructions for data input to the plotting program are given in Appendix II..

Input Data

Essentially, the required input consists of the grid geometry, flow parameters and initial data for the entire grid. A complete card file input description is given in Appendix II..

The first step in choosing the grid configuration is the location of the boundaries of the numerical calculations. As outlined in the section on boundaries, the upstream boundary is placed about five boundary layer thicknesses upstream of the base, the downstream boundary is placed at a location where the flow is expected to have returned to completely supersonic and the upper boundary is located so that it is in a completely inviscid flow regime. In picking a mesh size it must be remembered that the object is to compute flow fields of interest with as much accuracy as possible. Since the spatial stability is dependent upon the Reynolds number per mesh (Re_Δ), too large a value causes the program to fail. Therefore, the use of a coarse mesh requires a restriction of the magnitude of the free stream Reynolds number (Re_∞), in order to limit Re_Δ. On the other hand, the interesting features of the flow, such as the recirculation region, tend to be stretched out over a greater area as Re_∞ is increased. This shows the opposing effects of trying to have the recirculation region large enough to be observable, which requires large Re_∞, and trying to use a coarse

mesh to cut running costs, which requires a lower Re_∞ to give spatial stability. Furthermore, the grid must be fine enough to resolve the resulting flow field (e.g., the gradients in the body boundary layer). The axial step size is usually taken larger than the radial since smaller gradients are expected in the axial direction. Care must be exercised in using the variable mesh feature since the magnitude of α or β affects the order of accuracy of the difference formulas (Eq. (4)). The final configurations must represent a compromise between these considerations.

The flow conditions are described by specifying the free stream (ahead of shock) Mach number, Reynolds number, $\bar{M}_\infty = u_\infty^2/e_\infty$, γ_∞, Pr_∞ and for the constant wall temperature case, e_w/e_∞ (see Appendix II). It is also necessary to give the values of the four independent variables on the upstream boundary and the flow deflection along the upper boundary.

To start a calculation, initial values of each independent variable must be known for each grid point at which the finite difference equations are applied. The very first time a case is run a guess is made for this data. This can be based on the given upstream data, a known inviscid flow field or can be a uniform flow, etc. In practice, the computation is run for a set number of time steps, and the results observed. Then another series of time steps is run using the results of the previous computation as initial data. Means of doing this are described in Appendix II. When it is desired to vary flow parameters, say Re_∞, it is advantageous to start from some intermediate step in a previously run case whose Reynolds number is closest to the desired. Also, if a finer mesh is desired, the output from a coarse mesh run can be interpolated

and used as initial data. The machine output at the steady state condition has the same form as the initial data as described in Appendix II.

Time Step and Steady State Criteria

The time step size is related to the spatial mesh size by the stability condition. Normally there are two stability conditions, however, it is assumed that the differencing scheme used here has eliminated the viscosity dependent condition. An approximation to the other stability condition can be obtained by considering the differential equations with inviscid terms only and linearizing them. Following the procedure of Allen[4] the axisymmetric stability condition is

$$\Delta t \leq \frac{1}{2}(1+\beta)\ \Delta r \Big/ \left\{ \left(\frac{1+\beta}{1+\alpha}\right) \frac{\Delta r}{\Delta x} |u| + |v| + \frac{1}{M_\infty} \frac{(1+\beta)}{(1+\alpha)} \frac{\Delta r}{\Delta x} \left[1 + \left(\frac{\Delta x}{\Delta r}\right)^2 \left(\frac{1+\alpha}{1+\beta}\right)^2\right]^{\frac{1}{2}} \left[\gamma Xe/\gamma_\infty\right]^{\frac{1}{2}} \right\} \qquad (52)$$

Equation (52) is computed for each point at each step of the iteration. To be sure of stability, the program uses a Δt equal to 85% of the minimum value obtained from Eq. (52). For the coarse mesh (170 points), $\Delta t \approx 0.13$ to 0.14, while for the fine mesh cases (2040 - 3040 points), $\Delta t \approx 0.03$ to 0.04.

The solution is assumed to have reached the desired steady state when the density changes by less than a small number ϵ between successive time steps as given by Eq. (12). For the cases considered here, $\epsilon \sim 10^{-5}$ was found satisfactory.

Numerical Examples

The computer program for a spherically capped cylindrical body was run initially with a coarse mesh grid for various Reynolds number flows. Even though they lack accuracy these coarse mesh runs, which are relatively inexpensive, can be used to learn much about the program's limitations, such as maximum Reynolds number for a given mesh size, before running the more expensive fine mesh cases.

All the cases considered had a free stream Mach number, $M_\infty = 12.5$, $u_\infty^2/e_\infty = 78.8$, $\gamma = \gamma_\infty = 1.3$, and $e_w/e_\infty \simeq 6$ for constant wall temperature cases. The Reynolds number, Re_∞, was varied between 40 and 10,000 and two values of the Prandtl number were used, $Pr = Pr_\infty = 1.0$ and 0.72. An independent inviscid characteristics calculation was used to obtain the upper boundary flow deflection and the inviscid portion of the upstream boundary line. A boundary layer calculation[6] was made to complete the upstream data requirements.

It should be noted that all dimensions are in terms of the base half height or cylinder radius, and ∞ refers to the uniform conditions outside the bow shock. The lower Reynolds number cases were treated with a coarse grid having 170 points, while a fine mesh having 2040 points was used for the larger Reynolds numbers.

Coarse Mesh Solutions : The first runs were made with a coarse grid for the constant wall temperature conditions. A low Reynolds No.case, $Re_\infty = 40$ was used to see if convergence to a steady state solution was obtainable. A steady state was approached for this case after many parameter adjustments required in getting familiar with the program operation. However, for this coarse mesh the recirculation region was not observable. Therefore, a

case for Re_∞ = 400 was run. A converged solution was obtained but the recirculation region was still not evident. A run was then made with Re_∞ = 1200. This solution converged and showed a definite recirculation region. This is evidence of the mesh size tradeoff mentioned previously. If the Reynolds number is kept small to insure stability for a coarse mesh, which is cheaper to run, the recirculation region will be small and the coarse mesh will not intercept it. It should be mentioned that some of these coarse mesh runs have small negative density values behind the base. These seem to be localized and do not affect the rest of the flow field. They tend to disappear as steady state is approached, especially for the finer mesh cases.

Once it was established that a recirculation region could be obtained, the next step was to increase the Reynolds number to find the limit for which a solution could be obtained for the coarse mesh. After an Re_∞ = 1800 case was run to convergence a value of Re_∞ = 4000 was attempted. For this later case it was not possible to obtain a steady state condition. The calculation terminated itself when the internal energy became negative in a small region of the grid. This is a positive definite quantity for which negative values are unacceptable. All computations for which steady state solutions could not be reached were terminated in this manner. Subsequently, a case with Re_∞ = 2500 was run. This case also failed, giving a limiting Re_∞ of between 1800 and 2500 for coarse grid.

Since the terminating factor appears to be negative internal energy it would seem likely that the upper limit of Re_∞ could be increased by increasing the effect of the energy dissipation terms. This was investigated by reducing the Prandtl number, which appears in the denominator of these terms, from 1.0 to 0.72. When the

Re_∞ = 2500 case was rerun for Pr = 0.72, a converged solution was obtained. This was also true for Re_∞ = 3000; however, an Re_∞ = 3500 case failed. Therefore, the Reynolds number limit for a given mesh can be increased by enhancing the effect of the energy dissipation terms. All subsequent calculations were run with Pr = 0.72. Many additional partial runs with different Reynolds numbers and coarse grid arrangements were initiated in the course of the learning process. These are not reported here since they do not lead directly to any conclusions.

Fine Mesh Solutions: The coarse grid cases discussed above cannot be expected to give accurate results. They have been used to investigate the feasibility of obtaining solutions and the nature of the breakdown at large Reynolds numbers. In order to obtain a usable solution a fine mesh of 50 x 50 points was considered. Due to the body location there are actually only 2040 computation points. Running times to reach steady state for this mesh depend upon initial data but were between 1 and 1-1/2 hours for the cases considered. The initial case run on this mesh was the largest Reynolds number case obtained for the coarse mesh; Re_∞ = 3000. A convergent solution was obtained.

An analysis of Burgers' equation in one-dimension shows that for local Reynolds numbers, based on step size, greater than 2.0, the numerical solution exhibts point-to-point oscillations. However, for our more complex system and geometry, this does not seem to be true. Point-to-point oscillations do arise, however, for this Re_∞ = 3000 fine mesh case, and accompany large curvatures in the solution.

Figure 6 presents radial plots of the density at stations upstream of the corner. The solid curve without circles is the upstream starting profile, and the circles represent computed points somewhat downstream. In the left hand curve for constant wall temperature, the computed points show point-to-point oscillations near the body surface even though $Re_{\Delta r}$ is smaller there than at larger values of r. However, in the range of radius r where oscillations occur, the starting profile and the computed profiles have large curvatures. It was therefore concluded that point-to-point oscillations can occur when the mesh is not fine enough to represent curvature or local changes in a variable.

To check this conclusion, an adiabatic-wall case, which has a smoother density profile, was run. The right hand side of Figure 6 shows that no oscillations are present. The values of $Re_{\Delta r}$ in this case were small, and in order to further verify the dependence of oscillations on large curvatures the same case was run at a larger free-stream Reynolds number (10,000 instead of 3,000). This computation and the results appear in Figure 7. Now $Re_{\Delta r}$ is large but no oscillations exist since the curvatures are small.

Figure 8 shows the axial variation of density just above the body surface. The upper curves are for the constant wall temperature case and show oscillations, evidently remnants of the radial oscillations. The two curves show the time evolution of the solution. The lower curves are for the adiabatic wall, Re_∞=10,000 case and show only slight oscillations even though values of $Re_{\Delta r}$ are about the same as for the constant T_w case.

Figure 9 shows radial plots of density and internal energy for the constant T_w case at a location one half height behind the base. The density oscillations present in the body boundary layer

have propagated downstream. The adiabatic wall, Re_∞ = 10,000 case is plotted in Figure 10 at the same station and contains no oscillations. The time evolution of ρ is also indicated. Figure 11 is a similar plot for the adiabatic wall, Re_∞=10,000 at a station one diameter behind the base.

Figures 12, 13 and 14 are additional machine plotted results (see Appendix II) of the adiabatic wall, Re_∞=10,000 case. Figure 12 gives streamline contours. The recirculation region is well defined by the closed contours, which are plotted at finer increments of the stream function than the outer flow. The stagnation point is indicated by the intersection of the zero streamline and the flow center line (r = 0).

The lines in Figure 13 represent the velocity vectors throughout the computed field. Each vector starts at the small cross, each of which represents a grid point. The stagnation point is represented by the asterisk.

Machine-plotted pressure contours are shown in Figure 14. The convergence of the contours at the downstream end of the calculation field evidently represents the formation of a recompression shock.

The increasing of Re_∞ from 3,000 to 10,000 caused the Mach number at the downstream end of the grid to become subsonic. Hence a computation with a longer domain (50 x 70) was carried out to insure supersonic flow at the downstream boundary. The results in Figures 15 and 16 show that the curves plotted for the short-domain calculation are only slightly affected.

SUMMARY

GASL has developed a computer program which treats the near wake of an axisymmetric body having a truncated cylindrical base. The numerical approach is a two-step time-dependent finite difference procedure for the compressible Navier Stokes equations.

The program has the following features:

1) Axisymmetric flow field.
2) The calculated flow field includes the region upstream of the base where corner effects are present.
3) The inviscid flow along the outer horizontal boundary may be nonuniform.
4) A variable mesh is used to allow higher resolution in areas of flow nonuniformities.
5) Variable viscosity and conductivity are admitted.
6) Options of adiabatic wall or fixed wall temperature are admitted.
7) Both the equation system and the finite differencing are done in conservation form.
8) The stability condition for the time-dependent solution is independent of the viscosity (Cheng-Allen scheme).
9) Difference forms at the boundaries are obtained by means of telescoping with the internal difference forms.

A number of numerical examples have been run. Calculations using a coarse grid have shown that for small Reynolds numbers, where the recirculation region is small, the recirculation region may not be intercepted by the grid. For larger Reynolds numbers the recirculation region becomes evident, however, a limit of Reynolds number is reached for which a given grid size will not yield a convergent, steady state solution. This upper Reynolds number limit can be increased by enhancing the effect of the energy dissipation; by decreasing the Prandtl number, for instance.

Point-to-point oscillations in fine mesh solutions do not necessarily arise when the local Reynolds number, based on step size, is greater than 2.0 as is the case for the one-dimensional Burger's equation. However, such oscillations do arise when the mesh is not fine enough to accurately represent curvatures in the solution variables. This was verified by obtaining smooth solutions for an adiabatic wall case, with small variable curvatures, for either the same free stream Reynolds number or local Reynolds number per mesh as a constant wall temperature case with large curvatures, which exhibited oscillations.

REFERENCES

1. Brailovskoya, J. Y., "A Difference Scheme for Numerical Solutions of the Two-Dimensional, Nonstationary Navier-Stokes Equations for a Compressible Gas," Soviet Physics, Doklady 10, pp. 107-110, 1965. Translated from Doklady Akademii Nauk SSSR, 160, pp.1042-1045, 1965.

2. Dufort, E. C. and Frankel, S. P., "Mathematical Tables and Other Aids to Computation," Vol. 7,p. 135.

3. Cheng, S., "Accuracy of Difference Formulation of Navier-Stokes Equations," The Physics of Fluids, Supplement II,1969, pp. II-34 - II-41.

4. Allen, J. S., "Numerical Solutions of the Compressible Navier-Stokes Equations for the Laminar Near Wake in Supersonic Flow," Ph.D. Thesis, Dept. of Aerospace and Mech. Sci., Princeton Univ., 1968.

5. Allen, J. S. and Cheng, S. I., "Numerical Solutions of the Compressible Navier-Stokes Equations for the Laminar Near Wake," The Physics of Fluids, 13, 1970, pp. 37-52.

6. Lieberman, E., Lane, F. and Fox, H., "Analysis and Computer Program for Calculation of Non-Similar Laminar Boundary-Layer Properties: Air in Chemical Equilibrium and Finite Rate Chemistry," Picatinny Arsenal Technical Report 3565; AMC-67-22. GASL TR-660, June 1967.

7. Lax, Peter and Wendroff, Burton, "Systems of Conservation Laws," Comm. Pure and Applied Math., XIII, pp. 217-237, 1960.

8. Anderson, J. L., Preiser, S. and Rubin, E. L., "Conservation Form of the Equations of Hydrodynamics in Curvilinear Coordinate Systems," J. of Computational Physics, 2, 1968, pp. 279-287.

9. Ferri, A., "The Method of Characteristics," in General Theory of High Speed Aerodynamics, Ed. W. R. Sears. Princeton University Press, 1954, Princeton, New Jersey.